The Determination of the Location of Contact Electrification-Induced Discharge Events†

Sarah J. Vella,‡ Xin Chen,‡ Samuel W. Thomas III,‡ Xuanhe Zhao,§ Zhigang Suo,§ and George M. Whitesides*,‡,∥

Department of Chemistry and Chemical Biology, Harvard University, Cambridge, Massachusetts 02138, School of Engineering and Applied Sciences, Harvard University, Cambridge, Massachusetts 02138, and Wyss Institute for Biologically Inspired Engineering, Harvard University, Cambridge, Massachusetts 02138

Received: August 19, 2010; Revised Manuscript Received: September 9, 2010

This paper describes a method for determining the location of contact electrification-induced electrical discharges detected in a system comprising a steel sphere rolling in a circular path on an organic insulator. The electrode of the "rolling sphere tool" monitors, in real time, the separation of charge between the sphere and the organic insulator and the resultant electrostatic discharges. For every revolution of the sphere, the electrometer records a peak, the height of which represents the amount of charge on the sphere. As the charge on the sphere accumulates, the resulting electric field at the surface of the sphere eventually exceeds the breakdown limit of air and causes a discharge. The position of this discharge can be inferred from the relative amplitudes and positions of the peaks preceding and following the discharge event. We can localize each discharge event to one of several zones, each of which corresponds to a geometrically defined fraction of the circular path of the sphere. The fraction of charge on the sphere that could be detected by the electrode depended on the relative positions of the sphere and the electrode. The use of multiple electrodes improved the accuracy of the method in localizing discharge events and extended the range of angles over which they could be localized to cover the entire circular path followed by the sphere.

Introduction

Contact electrification—the transfer of charge between two objects when they are brought into contact and then separated—is ubiquitous;[1,2] even two pieces of identical material brought into contact can result in charge separation.[3−9] The phenomenon of contact electrification has been known for thousands of years[10] and has been exploited in many ways, including X-ray generation,[11] xerography,[12] and electrostatic separation.[13] A detailed understanding of the fundamental mechanism of contact electrification, however, has remained elusive. For example, contact electrification is often associated with friction ("rubbing a plastic comb with a silk scarf"); it is, however, presently unclear whether there are important differences between electrification with and without friction or whether friction is incidental to the pressures required to bring surfaces into intimate contact.[14]

The most significant result of contact electrification is the charge that develops on the participating surfaces. The amount of charge is dictated by the interplay between two counteracting processes: charging and discharging. With insulators, the former refers to the slow accumulation of charge by transfer of ions (and/or other charge carriers) from one surface to another (Figure 1a), and the latter is the rapid, localized discharge (probably mediated by a plasma or corona) between the two surfaces when the accumulated electric field exceeds the breakdown limit of the surrounding media (often air).[15]

Charging. The mechanism of charging between different classes of materials is still incompletely understood and is the subject of active debate.[16−22] Two mechanisms have been proposed for charge transfer between different materials: (i) electron transfer and (ii) ion transfer. Contact charging between conductors or semiconductors certainly can occur by electron transfer; these materials have mobile electrons and well-defined Fermi levels.[2] (The existence of a plausible mechanism for electron transfer does not, however, preclude charging by ion transfer.) In the earlier physics literature, many discussions

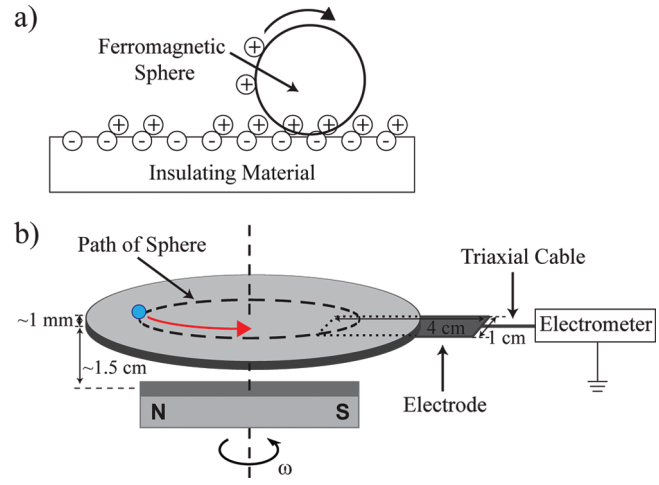

Figure 1. (a) Schematic illustration of a steel sphere rolling on a surface functionalized with covalently bound negative ions and mobile positive counterions; the mobile cations transfer to the sphere during contact electrification. (b) Illustration of the rolling sphere tool (RST) that measures the dynamics of contact electrification and electrical discharge. The RST system consists of a ferromagnetic sphere that rolls (not slides) in a circular path on an insulating material under the influence of a rotating magnet located below the surface. As the sphere rolls on the surface, charge separation occurs; an electrode located directly below a portion of the insulating material, and connected to an electrometer, records charge separation in real time.

† Part of the "Mark A. Ratner Festschrift".

* To whom correspondence should be addressed. E-mail: gwhitesides@gmwgroup.harvard.edu.
‡ Department of Chemistry and Chemical Biology.
§ School of Engineering and Applied Sciences.
∥ Wyss Institute for Biologically Inspired Engineering.

10.1021/jp107883u
Published on Web 09/29/2010

concerning charging of insulating materials have, however, assumed without (so far as we can see) any compelling experimental evidence that electron transfer is involved, even though there are neither plausible electron donors nor plausible acceptors in insulating organic solids. In any event, if free electrons were generated (as we believe they are during discharge events), they would attach themselves to molecules and form ions. Putterman et al. proposed that X-rays generated by the peeling of tape at reduced pressure were caused by electrons from electrostatic discharges that struck the positively charged adhesive.[11,23] Although some efforts to support the hypothesis of electron transfer (with data from an organic insulator in contact with a metal) have shown a correlation between surface charge density and work function of a metal,[24] others have shown that there is no correlation.[25] Bard and co-workers[17,18,26] have recently shown that vigorous rubbing of Teflon against, for example, poly(methylmethacrylate) (PMMA), induced apparent redox reactions (e.g., metal-ion reduction) on the surface of the charged Teflon when it was submersed in aqueous solutions containing appropriate redox agents. On the basis of these observations, they have suggested the involvement of something they called a "cryptoelectron" in contact electrification. It is, however, not clear what a "cryptoelectron" might be; the only possibilities for carriers of charge are electrons or ions. Gryzbowski and co-workers proposed an entirely different interpretation for similar phenomena. They attributed the reduction of metal ions and the bleaching of dyes by PDMS (charged either negatively or positively by contact electrification) to radicals generated by mechanical deformation on the surfaces of the polymers.[27,28]

Diaz and co-workers[29] proposed an ion-transfer mechanism for charge separation involving insulators. They investigated ionomers, a class of polymers comprising ions covalently bound to the polymer chain and unbound counterions. These polymers charged with the same sign as the covalently bound ion, whereas the contacting metal developed the charge of the mobile counterion (Figure 1a). In previous work,[30] we showed that the agitation of poly(styrene) microspheres functionalized with covalently bound, positively charged groups (with mobile negative counterions) developed a positive charge when they charged by contact electrification against an aluminum dish. Conversely, the agitation of poly(styrene) microspheres functionalized with covalently bound, negatively charged groups (with mobile positive counterions) charged negatively by contact electrification against an aluminum dish. More recently, we reported similar results for glass silanized with ionic, self-assembled monolayers.[31] All of these observations are consistent with the ion-transfer mechanism of charge separation for organic insulators.

Discharging. Unlike charging, discharging is sudden (~10 ns)[32] and quasi-periodic. As charge on an object accumulates due to contact electrification, so does the associated electric field. A discharge happens when this field exceeds a threshold, which is largely dictated by the dielectric strength[33] of the surrounding medium. Electrical discharge can be as powerful as lightning during thunderstorms or as trivial as sparking when touching a doorknob with a dry hand; the magnitude of the discharge depends mostly on the amount of charge transferred during the process. The factors that influence discharging are not well-understood and are also the subject of active research.[34,35]

Electrical discharges due to triboelectrification are estimated to cause billions of dollars in damages in the U.S. each year[36,37] in the forms of, for example, damage to electronic equipment[38] and damage from explosions caused by the ignition of combustible materials.[39] Understanding the factors that influence the probability of discharge will contribute to a fundamental understanding of the charging and discharging that characterize contact electrification, as well as to the development of strategies to control the likelihood and/or location of discharges, and thus to minimize the risk of sparking.

Rolling Sphere Tool. One of the difficulties in studying contact electrification, both charging and discharging, has been the lack of a reliable experimental system that can generate highly reproducible results. Grzybowski et al. first described a system that has proved exceptionally useful in studying tribocharging—the "rolling sphere tool" (RST) (Figure 1b).[40−42] This experimentally convenient system comprises a ferromagnetic steel sphere rolling (not sliding) on an insulating surface under the influence of a magnet rotating *under* the surface (with no direct, physical contact to it). The sphere follows a circular path on this surface. We have exploited the RST to study different aspects of contact electrification, including the mechanism and kinetics of charge separation,[40,41] the patterns of electrostatic charging and discharging,[31] strategies to control charging due to contact electrification,[43] and the dynamic self-assembly of charged spheres.[44] More recently, Thomas and Friedle used the RST to demonstrate control over charging behavior using photochromic polymers.[45]

This paper focuses on electrostatic discharge resulting from contact electrification. In a previous paper, we showed that the RST can reliably produce a large number of discharge events.[31] Here, we describe a method that we developed to determine the location of each individual discharge event. This method allowed us to perform statistical analysis on the positional distribution of discharges. In particular, we show that air plasma treatment of a surface can greatly influence the probability of discharge and that, if only a portion of surface was treated, we can locate that region using our method.

Experimental Design

The RST (Figure 1b) consists of a rotating permanent magnet, located ~1.5 cm below a disk made of an organic insulator (or any other dielectric material), the magnetic field of which causes a ferromagnetic stainless steel sphere to roll in a circular path on the disk.[44] An electrode (width = 1 cm, length ~ 4.0 cm, thickness ~ 100 μm) located directly *beneath, in contact with,* the disk (i.e., taped to the underside of the disk with electrical tape), connected to an electrometer (Keithley 6514), senses charge inductively in real time. The spinning magnet makes no measurable contribution to the charge measured in the system (see Figure S1, Supporting Information).

We used glass disks or poly(styrene) Petri dishes for the dielectric surfaces; they had thicknesses of ~ 1 mm. Glass disks were cleaned by washing them by hand with Micro-90 aqueous cleaning solution, rinsing them with water, and immersing them in a piranha solution (1:4 (v/v) 30% H_2O_2 (aq)/H_2SO_4) for 2 h. (CAUTION: Piranha should NOT be exposed to organic material! The peroxide should be added to the sulfuric acid very slowly. Piranha is extremely corrosive and potentially explosive!) The disks were then rinsed with ~50 mL of deionized water (Millipore) and ~50 mL of 95% ethanol and dried at 60 °C under vacuum overnight. VWR brand Petri dishes were used as received.

Figure 2 plots the accumulation of the charge measured by the electrometer in time. The measured charge consisted of two parts: the charge on the *sphere* (Q_s) and the charge on the portion of the *disk that is near the electrode* (Q_{dne}) and close enough for it to be inductively coupled to the electrode. Peaks in the

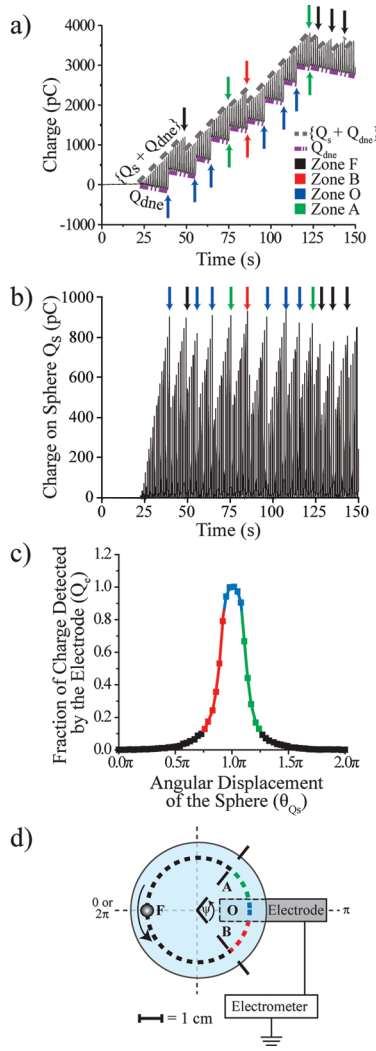

Figure 2. (a) Experimental data showing the charge sensed by the electrode during contact electrification of a steel sphere ($d = 3.2$ mm) rolling on a glass disk ($T \sim 25$ °C, RH < 10%). The width of the electrode (w) was 10 mm (0.13π rad), and the circumference of the circle traced by the sphere was ~150 mm. Electrical discharge events (indicated by arrows) interrupted the linear accumulation of charge in the baseline (which represents the charge on the area of the disk close to the electrode) [Q_{dne}, purple (-•••-)], and/or in the peaks (which represent the sum of net charge on the sphere and the surface of the glass disk near the electrode) [{$Q_s + Q_{dne}$}, (---)], or a combination of both. Blue arrows indicate discharges that occurred close to, or over, the electrode, black arrows indicate discharges that occurred sufficiently far from the electrode that the electrode did not sense them, red arrows indicate those that occurred just before the sphere rolled over the electrode, and green arrows indicate those just after the sphere rolled over the electrode (vide infra). (b) Processed data showing only Q_s (=[{$Q_s + Q_{dne}$} − Q_{dne}) sensed by the electrode. The colored arrows correspond to the same discharges shown in (a). (c) A plot of Q_s over one period (one revolution of a steel sphere rolling on a poly(styrene) (PS) Petri dish). $Q_s = \{Q_s + Q_{dne}\} - Q_{dne}$ and was normalized to 1. The curve represents the fraction of charge on the sphere that the electrode detected (black segment, 0−0.1; red and green segments, 0.1−0.9; blue segment, 0.9−1.0) as a function of the position of the sphere relative to the center of the electrode (width, $w = 1.0$ cm); we assigned the center of the electrode to be π radians. (d) The circular path of the sphere was divided into four detection zones: Zone F, the sphere is far from the electrode (black); Zone B, the sphere is near the electrode, approaching it (before the electrode) (red); Zone O, the sphere is directly over the electrode (blue); and Zone A, the sphere is near the electrode, moving away from it (after the electrode) (green). Each zone corresponds to the colored segment in (c). The arrow indicates the direction in which the sphere rolled.

data occurred when the sphere was directly above the electrode; for these peaks, the electrometer measured the sum of the charge on the sphere and the portion of the disk near the electrode ({$Q_s + Q_{dne}$}). Valleys occurred when the sphere was far from the electrode; at the floor of these valleys, the electrometer measured only the charge on the portion of the disk that the electrode sensed (Q_{dne}). In this example, the sphere charged positive and the surface charged negative.[46]

Charge separation between the sphere and the disk produced a potential difference that eventually led to electrical discharge. In Figure 2, each discharge event corresponds to a sharp disruption in the trend lines characterizing the data (e.g., those indicated by arrows). Sudden decreases in the heights of the peaks ($\Delta\{Q_s + Q_{dne}\}$) or sudden increases in the baseline (ΔQ_{dne}), or by a combination of both, characterized these disruptions.

Processing the data by subtracting Q_{dne} from {$Q_s + Q_{dne}$} (eq 1) generated a plot that showed only Q_s (the charge the electrode sensed on the sphere) versus time (Figure 2b). From these data, we obtained the maximum amount of charge on the

$$Q_s = \{Q_s + Q_{dne}\} - Q_{dne} \quad (1)$$

sphere before and after each discharge. The difference between them (ΔQ_s) gave the total amount of charge transferred during a discharge (eq 2).

$$\Delta Q_s = Q_s \text{ (before discharge)} - Q_s \text{ (after discharge)} \quad (2)$$

Table 1 summarizes the variables (and their meanings) that appear throughout the paper.

The average maximal charge on a steel sphere ($d = 3.2$ mm) rolling on plasma-oxidized poly(styrene) before discharge in air was 1250 ± 380 pC. This value is on the same order of magnitude as the value of 940 ± 60 pC determined from a steel sphere of the same size rolling on clean glass.[31] The electric field at the surface of an isolated sphere is given by eq 3:

$$\vec{E} = \frac{Q}{4\pi\varepsilon_0 r^2} \quad (3)$$

A steel sphere ($r = 1.6$ mm) with a charge of 1250 pC has an electric field of ~44 kV/cm at its surface; this value is close to the dielectric strength of air (~30 kV/cm at 1 atm of pressure). Our earlier results also showed that the maximal charge that accumulated on the steel sphere before discharge correlated with the dielectric strength of the surrounding gas.[31]

Results and Discussion

Division of the Path of the Sphere into "Detection Zones" Based on the Fraction of Charge on the Sphere that the Electrode Detected (Q_e). We divided the circular path of the sphere into four "detection zones"—parts of the trajectory of the sphere to which we could assign a discharge event—based on the fraction of charge on the sphere (Q_e) that the electrode detected (Figure 2c): (i) Zone F, the section of circular path sufficiently far from the electrode that the electrode did not sense the charge on the sphere (<10%); (ii) Zone O, the section of circular path where the sphere was directly over the electrode and the electrode sensed 90−100% of the charge on the sphere; (iii) Zone B, the section of circular path just before the electrode,

TABLE 1: Summary of the Variables That Appear Throughout the Paper and Their Meanings

symbols or variables	unit	value	also represents
Q_s	pC	charge on the sphere	
Q_d	pC	charge on the entire disk	
Q_{dne}	pC	charge on the disk near the electrode	baseline
$\{Q_s + Q_{dne}\}$	pC	charge on the sphere and the disk near the electrode	peaks
$\Delta\{Q_s + Q_{dne}\}$	pC	change in charge in the peaks in one discharge event	peak disruption
ΔQ_{dne}	pC	change in charge on the disk near the electrode in one discharge event	baseline disruption
ΔQ_s	pC	total amount of discharge in one discharge event	$\Delta\{Q_s + Q_{dne}\} + \Delta Q_{dne}$ peak disruption + baseline disruption
θ_{Q_s}	radians	angular position of the sphere w.r.t. the electrode	
Q_e	pC	charge that the electrode detected	
Ψ	radians	angular size of detection zones spanning zones B, O, and A	
$\Delta\{Q_s + Q_{dne}\}/\Delta Q_s$	pC	fraction of peak discharge in one discharge event	
$\Delta Q_{dne}/\Delta Q_s$	pC	fraction of baseline discharge in one discharge event	
φ	radians	angle between the plane of the electrode and the center of the sphere	

TABLE 2: Summary of the Angular Sizes of the Detection Zone Resulting from the Different Widths of the Electrodes

electrode width (cm)	angle Ψ of detection zones spanning zones B, O, and A	portion of circular path sensed by the electrode (radians)	fraction of circular path sensed by the electrode
0.5	86°	0.48π	0.24
1.0	97°	0.54π	0.27
2.0	124°	0.69π	0.34

where the sphere was approaching the electrode and the electrode sensed 10−90% of the charge on the sphere (depending on its angular distance from the electrode); and (iv) Zone A, the section of circular path just after the electrode, where the sphere was moving away from the electrode and the electrode also sensed 10−90% of the charge on the sphere. The layout of the four zones is shown in Figure 2d. The angular size of the detection zones (Ψ) depended on the width of the electrode;[47] Table 2 summarizes the fraction of the circular path that Zones B, O, and A covered, as determined by the width of the electrode.

The Peaks/Valleys Preceding and Following Each Discharge Event Indicated Its Location. Using the shape of the data trace around each discharge event, we determined in which of the four zones the discharge occurred (Figure 3). A discharge in Zone F deposited charge onto a portion of the insulating disk sufficiently far from the electrode that the electrode did not sense this deposited charge. The electrode did not sense the change in charge on the sphere until the sphere rolled over the electrode (∼half a period later than the discharge event). The electrometer then registered an abrupt decrease in $\{Q_s + Q_{dne}\}$: a disruption in the linear accumulation of the heights of the *peaks* of the data. We referred to this type of discharge as a "peak" disruption. One such example is shown in Figure 3a. No apparent disruption in the linear accumulation of Q_{dne} occurred in this case.

In contrast, a discharge in Zone O deposited charge onto a portion of the disk directly above the electrode. In this case, no change in charge was detected immediately because the total charge ($\{Q_s + Q_{dne}\}$) remained the same. The electrode did not sense the redistribution of charge until about half a period later when the sphere had moved away from the electrode; the electrometer then registered an increase in Q_{dne} (ΔQ_{dne}). An abrupt increase in Q_{dne} caused a disruption in the linear accumulation of the baseline in the data; we, therefore, referred to this type of discharge as a "baseline" disruption (Figure 3b). No apparent disruption in the linear accumulation of the peaks occurred in this case.

A discharge that occurred in Zone B transferred charge from the sphere to a region of the disk just *before* the electrode; the electrode sensed the decrease in $\{Q_s + Q_{dne}\}$ as the sphere rolled over the electrode and sensed the increase in Q_{dne} after the sphere rolled away from the electrode. As a result, the electrometer registered the redistribution of charge as a "peak" disruption, followed by a "baseline" disruption (Figure 3c).

A discharge that occurred in Zone A deposited charge on the disk in a region just *after* the electrode; the electrode first sensed the increase in Q_{dne}, then the decrease in $\{Q_s + Q_{dne}\}$, the reverse of the manifestation of a Zone B discharge. Figure 3d plots such an event featuring a "baseline" disruption, followed immediately by a "peak" disruption.

Statistical Analysis of the Distribution of Discharges. We tested our method by recording and analyzing 2998 discharge events registered in 14 experiments where a steel sphere (d = 3.2 mm) rolled on a plasma-oxidized PS Petri dish along a circular path with a circumference of ∼15 cm. We assigned 1952, 321, 320, and 405 discharges to Zones F, B, O, and A, respectively, which correspond to 65 ± 7, 11 ± 3, 11 ± 3, and 14 ± 5% of the discharges, respectively. These errors were weighted standard deviations. In principle, they should have the same values; therefore, we estimated the actual error to be ±5%. Because the dish is homogeneous, a random distribution of discharges would result in a percentage of discharges in a zone equal to the percentage of the path length in that zone. Under our experimental conditions—an electrode with a width of 1.0 cm and a total circular path of the sphere of 15 cm—Zones F, B, O, and A covered 73, 10, 7, and 10% of the circular path of the sphere, respectively. A random distribution would have resulted in 7% of the total number of discharges occurring over the electrode (Zone O). The statistical analysis shown above, however, reported that, on average, 11 ± 3% of the discharges registered in Zone O, not significantly higher, but possibly statistically higher, than that expected from a random distribution.

Experiments using electrodes of different widths produced similar observations; for 0.5 or 2.0 cm electrodes, the expected distributions for Zone O were 4% or 15%, respectively, yet the observed distributions were 6 ± 2% and 18 ± 3%, respectively (Figure 4).

The small deviation of the observed distribution of discharges from a random distribution in Zone O may reflect the sphere experiencing a larger electric field when it was over the electrode than when it was far from the electrode. Several possible factors might have contributed to this increased electric field. The image charge that developed on the electrode when the sphere was

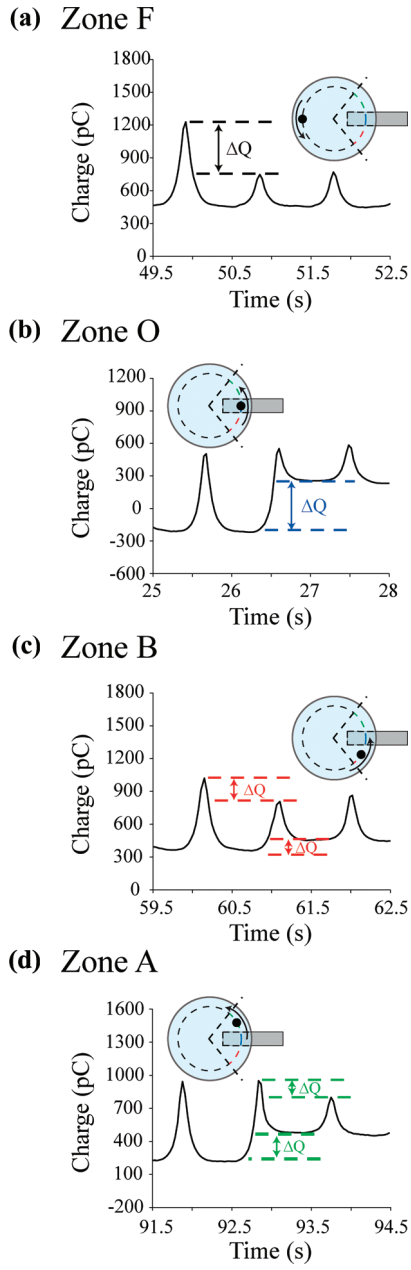

Figure 3. Sections of unprocessed data illustrating a discharge event located in a) Zone F - "*Peak*" disruption; b) Zone O - "*Baseline*" disruption; c) Zone B - "*Peak*" followed by "*Baseline*" disruption; d) Zone A - "*Baseline*" followed by "*Peak*" disruption.

over the electrode could have imposed a greater electric field at the surface of the sphere (see Figure S2, Supporting Information). A greater electric field at the edges of the electrode (higher local curvature) could also have contributed to the slightly skewed distributions that we observed.

Discharge Occurred Preferentially in Regions Exposed to Plasma Oxidation. We then studied substrates with a nonhomogeneous surface chemistry by treating a portion of the surface with an air plasma. These experiments had two goals: (i) to demonstrate that we could influence the location of discharges by modifying a surface and (ii) to prove that our experimental method can indeed detect such changes. Plasma oxidation of a PS Petri dish incorporates oxygenated functional groups, including carbonyl, carboxyl, and hydroxyl, onto the surface of the polymer.[48−51] We have shown before that such surfaces charge more rapidly than do those of unoxidized, nonpolar polymers

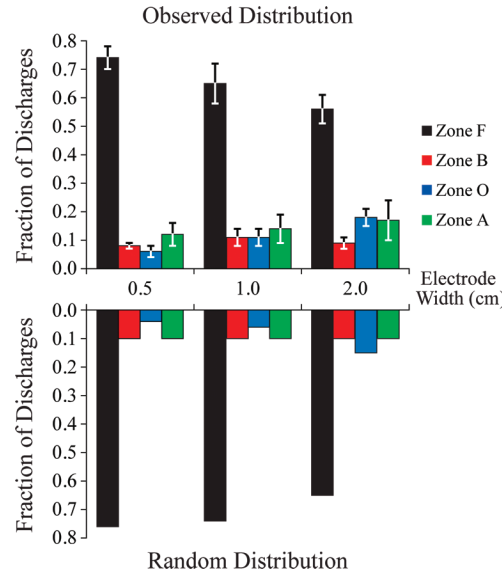

Figure 4. Comparison of the fraction of discharges that occurred in each zone for experiments (steel sphere, $d = 3.2$ mm, rolling on a plasma-oxidized PS dish) that used electrodes of different widths ($w = 0.5, 1.0, 2.0$ cm). Top: the observed distribution of discharges obtained from the evaluation of more than 1400 discharges for each size of electrode. These error bars represent weighted standard deviations as determined from a minimum of five experimental data sets for each electrode width. Bottom: the distribution of discharges that would be expected if they occurred randomly. The observed fractions of discharges for Zone O were slightly greater than what would be obtained if the distributions were random.

because of the increased density of ionizable species.[40] In our experiments, a sphere rolling on an untreated PS dish charged much more slowly (~10 ± 5 pC/s) than one rolling on an oxidized PS dish (~485 ± 250 pC/s). At the same time, the plasma-treated surface of PS accumulated more charge (with opposite polarity from the charge on the sphere) than the untreated surface. We expected the oxidized surfaces to discharge more often because they accumulated charge more rapidly.

We selectively exposed a region of the surface of a PS dish (ex. Zone B) to an air plasma for 1 min by covering the dish with a flat PDMS disk from which a section had been removed (Figure 5a). After plasma oxidation, the PDMS disk was removed.

Figure 5b summarizes the results obtained from such samples when either Zone B, Zone O, Zone A, or the entire surface was plasma-oxidized. For each different zone, we measured at least four different samples, and the number of discharges in each experiment was at least 75.[52] Analysis of the number of discharges in each zone for these experiments revealed that the majority of discharges occurred in the treated zone. We used the homogeneously plasma-treated PS (Figure 5b-iv) as a control with which to compare the discharge distributions obtained from the nonhomogenously treated samples. The oxidation of Zone B (Figure 5b-i) or Zone A (Figure 5b-iii) resulted in 66 ± 10% of the discharges in the corresponding zone, which is almost 7 times greater than the fraction of discharges observed for those zones when the entire surface of the PS dish was plasma-oxidized. Oxidation of Zone O resulted in 97% (450 of 462) of the discharges in that zone (Figure 5b-ii), a 10-fold increase from the homogeneous PS surface. Our method for determining the location of discharges proved that an easily executed modification to a surface can indeed affect where discharges occur.

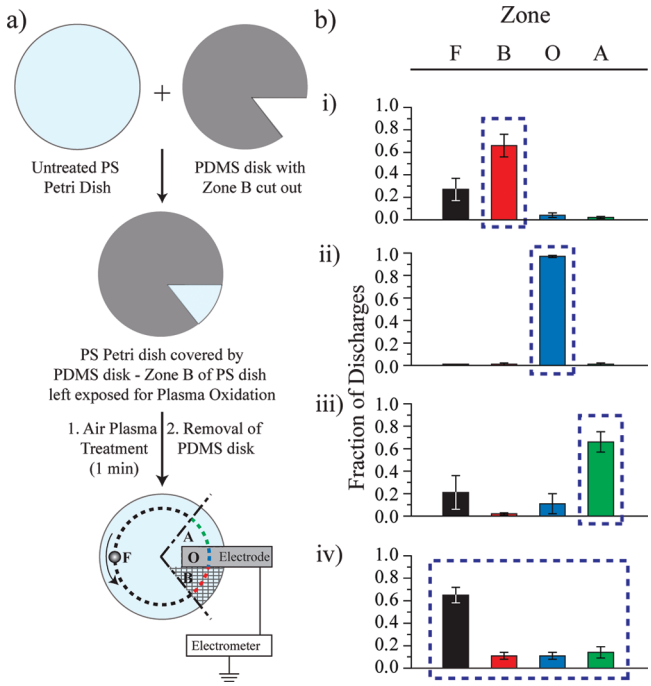

Figure 5. (a) Plasma oxidation of Zone B—indicated by the hatchmarks—of a PS Petri dish. (b) Summary of the fraction of discharges that resulted from a steel sphere ($d = 3.2$ mm) rolling on a PS Petri dish ($T \sim 25$ °C, RH < 10%) with (i) Zone B plasma-oxidized, (ii) Zone O plasma-oxidized, (iii) Zone A plasma-oxidized, and (iv) 100% of the disk plasma-oxidized. Dashed rectangles highlight the regions that were plasma-oxidized.

The Fraction of Charge that the Electrode Detected Depended on the Location of the Sphere. The electrode only sensed a fraction (from 0 to 100%) of the charge on the sphere Q_s, and that fraction depended on the angular position of the sphere relative to the electrode. We define $f(\theta)$ to be this fraction as a function of the angular position of the sphere (θ) with respect to the center of the electrode (the position that we assigned to be $\theta = \pi$ radians). The electrode only senses a fraction of the total charge on the disk, as well. We call the distribution of charge along the circular path $Q_d(\theta)$. Assuming that the function $f(\theta)$ is the same for both the sphere and the disk, the charge on the disk that can be sensed by the electrode is represented by eq 4. The total charge detected by the

$$Q_{dne} = \int_0^{2\pi} Q_d(\theta) f(\theta)\, d\theta \tag{4}$$

electrode (Q_e) is, therefore, the sum of a fraction of charge on the sphere $Q_s \cdot f(\theta)$ and Q_{dne} (eq 5). The disk, however, is stationary relative to the electrode, and the value of Q_{dne}

$$Q_e(\theta) = Q_s \cdot f(\theta) + Q_{dne} \tag{5}$$

does not change significantly with the position of the sphere in a given period. We, therefore, subtracted its contribution to Q_e (Figure 2c) to give eq 6.

$$Q_e(\theta) = Q_s \cdot f(\theta) \tag{6}$$

The function $f(\theta)$ can be determined from first principles. Integration of the electric fields from the sphere and the image charge ($\vec{E}_{tot}$) that passed through the surface of the electrode gave the charge induced on the electrode (eq 7) (for details, see the Supporting Information). Here, A is the surface area of the electrode, and ε_0 is the permittivity constant).

$$Q_e = \int_{\pi-w-\theta}^{\pi+w-\theta} \int_{-l}^{+l} A_{electrode}(\varepsilon_0 \vec{E}_{tot} dy\, dx) \tag{7}$$

We define the coordinate system with x and y axes in the same plane as the surface of the disk, and the z axis perpendicular to the surface of the disk. As a result of symmetry, only the z components of the electric fields of the sphere and its image charge have net contributions (the contributions of the other components cancel each other) (eq 8):

$$\vec{E}_z = \vec{E} \sin\phi = \frac{Qz}{4\pi\varepsilon_0 R^3} \tag{8}$$

Substituting eq 8 into eq 7 gives eq 9:

$$Q_e = \frac{Q_s z}{\pi} \int_{\pi-w-\theta}^{\pi+w-\theta} \int_0^{+l} \frac{1}{(z^2 + x^2 + y^2)^{3/2}} dy\, dx \tag{9}$$

Evaluating the integrals in eq 9 gave eq 10, where we made the approximations that the electrode was infinitely long relative to its width and that the dimensions of the electrode are significantly greater than those of the sphere (Figure S5 in the Supporting Information and eq 8). The Supporting Information details the derivation of eq 10.[40,53]

$$Q_e = \frac{Q_s}{\pi}\left[\arctan\left(\frac{\theta - \pi + w}{z}\right) - \arctan\left(\frac{\theta - \pi - w}{z}\right)\right] \tag{10}$$

In eq 10, Q_e is the fraction of charge on the sphere detected by the electrode, Q_s is the charge on the sphere just before discharge, θ is the angular position of the sphere (in radians) when discharge occurred (with respect to the center of the electrode, which was assigned to be π radians), w is the width of the electrode (in radians), and z is the vertical distance between the center of the sphere and the electrode.

In reality, our experiment setup did not have an infinitely large electrode. We chose to adapt the equation obtained from first principles (eq 10) and use adjustable parameters to fit one period (a single peak) of our experimental data (eq 11).

$$y = a\left[\arctan\left(\frac{\theta - \pi - b}{c}\right) - \arctan\left(\frac{\theta - \pi + b}{c}\right)\right] \tag{11}$$

In eq 11, y is the fraction of charge transferred to the disk during a discharge that the electrode detected, θ is the angular position of the sphere (in radians) when discharge occurred (with the center of the electrode assigned to be π radians), a is the fitting parameter corresponding to the height of the peak, b is the fitting parameter corresponding to the width of the peak (in radians), and c is the fitting parameter corresponding to the slope of the peak (in radians).

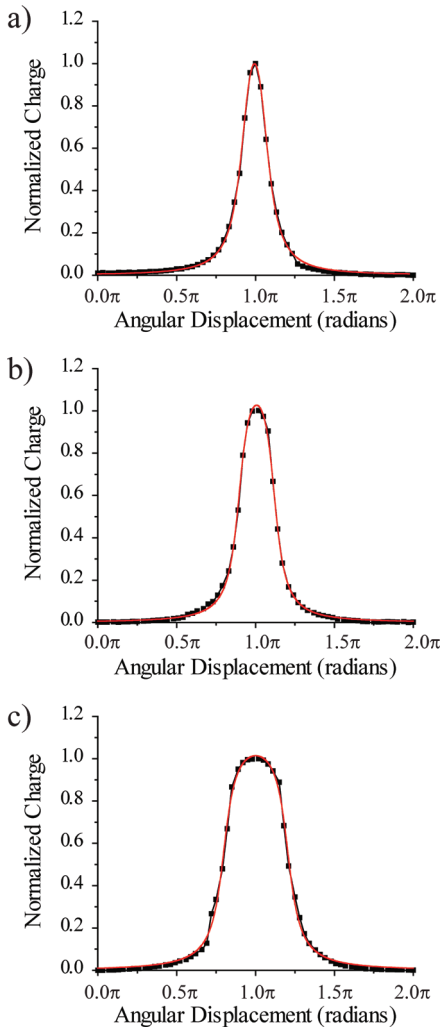

Figure 6. Graphs showing the comparisons between the nonlinear least-squares fit to eq 11 (solid red line) and the data (black -■-) collected using electrodes with widths of (a) 0.5, (b) 1.0, and (c) 2.0 cm. The fitting parameters are listed in Table 3.

TABLE 3: Values for the Fitting Parameters in eq 11 Obtained from Nonlinear Curve Fitting Models for Representative Peaks Obtained from Data Using 0.5, 1.0, and 2.0 cm Electrodes

electrode width (cm)	*a* (radians)	*b* (radians)	*c* (radians)
0.5	0.7	0.06	0.07
1.0	0.5	0.1	0.06
2.0	0.4	0.2	0.06

We fit a single peak from each set of data collected using electrodes with widths of 0.5, 1.0, or 2.0 cm to eq 11 (Figure 6). All sets of data displayed good fits. Table 3 gives the values of the variables obtained from nonlinear curve fitting models for representative peaks obtained from data using 0.5, 1.0, and 2.0 cm electrodes. We obtained the value of y at each discharge event from the data (the fraction of discharge contributed by the baseline disruption *is* the value of y (vide infra)) and used eq 11 to calculate the position of the discharge.

The Fraction of Discharge Representing the Amount of Baseline Disruption ($\Delta Q_{dne}/\Delta Q_s$) Identified the Location of a Discharge Event. We assumed that total charge was conserved during a discharge event. When the sphere discharged over the electrode, the electrometer detected an increase in Q_{dne}, but $\{Q_s + Q_{dne}\}$ did not change (and continued to increase

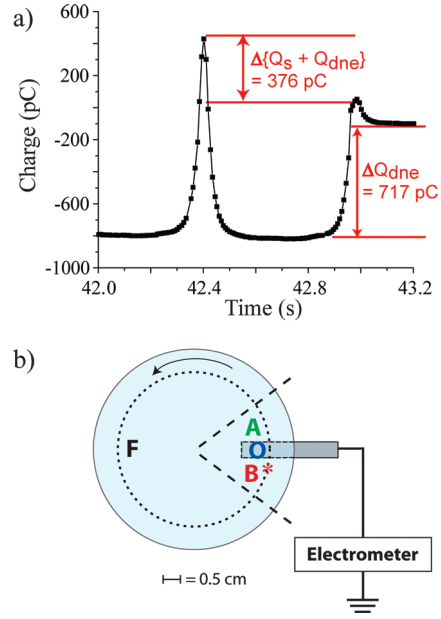

Figure 7. (a) A contact electrification-induced discharge between a steel sphere (d = 3.2 mm) rolling on a plasma-treated PS Petri dish using an electrode with a width of 0.5 cm ($T \sim 25$ °C, RH < 10%). The total discharge (ΔQ_s) was 1093 pC, of which 376 pC (34%) registered as a "peak" disruption ($\Delta\{Q_s + Q_{dne}\}$) and 717 pC (66%) registered as a "baseline" disruption (ΔQ_{dne}). (b) Illustration showing the location of the discharge at 0.92 π rad (marked by $*$).

linearly). In other words, $|\Delta Q_{dne}| = |\Delta Q_s|$. This experimental observation implies that charge was transferred from the sphere directly to the disk and that the total amount of charge was conserved during discharge. Importantly, none of the charge seems to be lost to the atmosphere during a discharge. When discharges happened in Zone B or A, we observed $|\Delta Q_{dne}| < |\Delta Q_s|$. Because the electrode checked the value of ΔQ_s at every revolution, such results indicated that only part of the charge that transferred from the sphere to the disk was detected by the electrode. Therefore, the value of $\Delta Q_{dne}/\Delta Q_s$ indicates the fraction of the charge that deposited onto the disk that the electrode sensed. This fraction corresponds to the position at which the discharge occurred, as indicated in eq 11. Discharges for which $\Delta Q_{dne}/\Delta Q_s < 0.1$ occurred in Zone F (Figure 3a). We could not determine the exact positions of these discharge events more precisely than assigning them to somewhere in this zone because experimental uncertainty in $\Delta Q_{dne}/\Delta Q_s$ is typically ~5%; this error is based on the uncertainty in determining the maximum charge on the sphere before and after a discharge.[54] For this reason, we referred to Zone F as the "zone of uncertainty". Discharges for which $\Delta Q_{dne}/\Delta Q_s > 0.9$ occurred in Zone O (directly over the electrode).

Discharges for which $0.1 < \Delta Q_{dne}/\Delta Q_s < 0.9$ were first assigned to Zone B or A. In Figure 3, we showed that we assigned the discharge to Zone B or A depending on the order of "baseline/peak" disruptions. Equation 11 allowed us to obtain the exact position of the discharge.

An example is shown in Figure 7, which shows the electrometer trace that reflects a discharge that occurred at $\theta = 0.92\pi$ rad from the center of the electrode. In this example, the electrometer recorded a "peak", followed by "baseline" disruption; therefore, this discharge occurred in Zone B (just before the electrode). The total discharge (ΔQ_s) was 1093 pC, of which 376 pC registered as a "peak" disruption ($\Delta\{Q_s + Q_{dne}\}$) and 717 pC registered as a "baseline" disruption (ΔQ_{dne}). The ratio of $\Delta Q_{dne}/\Delta Q_s = 0.66$ corresponded to the position at 0.92π

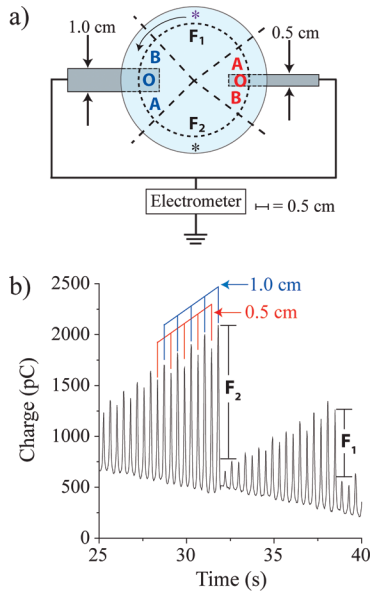

Figure 8. (a) Schematic representation of experiments using two electrodes (widths of 1.0 and 0.5 cm) positioned at π radians from each other and separated by 3.0 cm (1.5 cm from the center of the PS dish), with both electrodes connected to a single electrometer. Blue zones correspond to the 1.0 cm electrode, and red zones correspond to the 0.5 cm electrode. The arrow indicates the direction in which the sphere rolled. (b) Contact electrification of a steel sphere ($d = 3.2$ mm) rolling on a plasma-treated PS Petri dish ($T \sim 25$ °C, RH <10%). The first discharge shown occurred in Zone F_2 (∗), and the second discharge shown occurred in Zone F_1(purple ∗). The exact positions of the discharges cannot be assigned within Zones F_1 and F_2.

rad—indicated by the asterisk in Figure 7b—with respect to the center of the electrode.

The error in locating an individual discharge depended on where it happened. The ~5% error in determining $\Delta Q_{dne}/\Delta Q_s$ translates to an error in determining the location of a discharge, θ. The propagation of the error was nonlinear, but it varied with the position of the discharge. The error in θ was the greatest in Zone F. The error was the smallest in Zones B and A at the steepest part of the slope shown in Figure 2c where the calculated error was ca. $\pm 0.01\pi$ rad; this value is actually smaller than the diameter of the sphere ($d = 3.2$ mm, which is equivalent to 0.04π rad). We, therefore, estimated the error in θ in Zones B, O, and A to be equivalent to the diameter of the sphere (ca. $\pm\ 0.02\pi$ rad).

Using Multiple Electrodes Improved the Determination of the Location of Discharges. Using a configuration incorporating a single electrode, we had to assign a significant portion of the disk to Zone F (the zone in which the electrode did not sense any charge). This limitation in the sensitivity of the electrode prevented the quantitative assignment of the position of a discharge in Zone F (typically 70% of the path that was traced by the sphere). To improve the accuracy in determining the location of discharge events, we increased the number of electrodes. With an increased number of detection zones, we extended the amount of the circular path that could be sensed by the electrodes.

Two Electrodes, One Electrometer. Two electrodes (widths = 1.0 and 0.5 cm positioned at π radians from each other and separated by 3.0 cm) increased the number of detection zones from four to eight. A single electrometer recorded the output of both electrodes (Figure 8a), which were physically separated, but were electrically connected by a wire. It was necessary to use electrodes with different widths so that the position of the sphere with respect to each electrode could be distinguished by the widths of the peaks of the data. Electrodes with different widths produced peaks with corresponding widths; a peak recorded when the sphere rolled over the 1.0 cm electrode (fullwidth at half-height (fwhh) ~ 0.3π rad) was wider than a peak recorded when the sphere rolled over the 0.5 cm electrode (fwhh ~ 0.2π rad). "Uncertainty" zones (F_1 and F_2)—zones for which an exact discharge position cannot be determined beyond assigning a discharge zone—still existed in this configuration. The combined arc (1.0π rad) of the two uncertainty zones, however, was smaller than the arc of Zone F from the experiments with the single electrode (1.52π and 1.46π rad for electrodes with $w = 0.5$ and 1.0 cm, respectively). As examples, the two discharges shown in Figure 8b were both "peak" disruptions ($\Delta Q_{dne}/\Delta Q_s < 0.1$);[55] therefore, both discharges occurred in zones of uncertainty. The first discharge occurred in Zone F_2 and the second in Zone F_1.

Four Electrodes, Two Electrometers. To improve further the determination of the location of discharges along the circular path of the sphere, we used four electrodes connected to two electrometers. In these experiments, the configuration of electrodes consisted of a 2.0 cm electrode (E1_2.0) and a 1.0 cm electrode (E1_1.0) positioned at π radians to each other, separated by 3.0 cm, both connected to electrometer 1, and a 1.0 cm electrode (E2_1.0) and a 0.5 cm electrode (E2_0.5) positioned at π radians to each other, separated by 3.0 cm, both connected to electrometer 2 (Figure 9a). It was necessary to use electrodes with different widths in order to distinguish between the positions of the sphere on different regions on the disk. A peak recorded when the sphere rolled over the 2.0 cm electrode had a fwhh of ~0.4π rad, which was wider than peaks recorded when the sphere rolled over the 1.0 cm electrode (fwhh ~ 0.3π rad) or 0.5 cm electrode (fwhh ~ 0.2π rad).

The arc of the detection zone for the E2_0.5 electrode was 0.48π rad. The arc of the detection zones for each of the 1.0 cm electrodes was 0.54π rad. The arc of the detection zone for the E1_2.0 electrode was 0.69π rad. With this configuration, at least one of the electrodes detected the charge on the sphere at all points along the circular path of the sphere. We assigned the 16 zones as shown in Figure 9a. The detection zones of two adjacent electrodes overlapped and created a zone where both electrodes simultaneously detected the charge on the sphere or a discharge that occurred in that zone. Zones C, G, K, and O were the zones of overlap. Figure 9b highlights a section of data representing a discharge in the smallest zone of overlap, Zone K (zone of overlap between the E1_1.0 and the E2_0.5 electrodes). Electrometer 1 registered a "baseline" disruption, followed by a "peak" disruption, indicating that a discharge occurred after the sphere rolled over the E1_1.0 electrode. For this discharge, the total discharge (ΔQ_s) = 1005 pC and $\Delta Q_{dne}/\Delta Q_s = 0.23$. Electrometer 2 registered a "peak" disruption, followed by a "baseline" disruption, indicating that a discharge occurred before the sphere rolled over the E2_0.5 electrode. ΔQ_s measured by electrometer 2 for the E2_0.5 electrode was 1002 pC, and $\Delta Q_{dne}/\Delta Q_s = 0.04$. Using eq 11, we confirmed that the discharge occurred in Zone K at 1.36π rad with respect to the center of the E1_2.0 electrode (assigned as 0π rad).

Using the Multiple Electrodes Configuration to Identify and Locate a Plasma-Treated Region. Plasma oxidation does not make any visible changes to a surface because it only affects the first few nanometers of a surface; this shallow modification makes the chemical effects of plasma oxidation difficult to detect by common analytical techniques. SIMS and XPS are capable of detecting these changes, but they require expensive

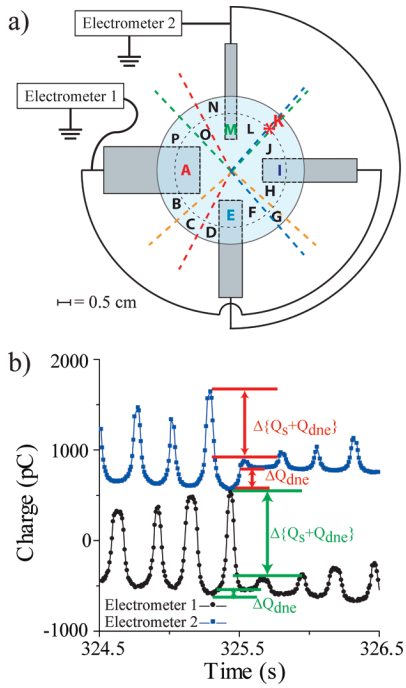

Figure 9. (a) Schematic representation of experiments using four electrodes, with widths of 2.0, 1.0, 1.0, and 0.5 cm, arranged at 0.5π rad from each other and 1.5 cm from the center of the Petri dish. Electrometer 1 measured the response from the π-radians separated 2.0 and 1.0 cm electrodes (black trace -•-); electrometer 2 measured the response from the π-radians separated 1.0 and 0.5 cm electrodes (blue trace -■-). (b) Contact electrification-induced discharge between a steel sphere (d = 3.2 mm) rolling on an air-plasma-treated PS Petri dish at ω = 112 rpm ($T \sim 25$ °C, RH < 10%). The total discharge (ΔQ_s) measured by electrometer 1 for the 1.0 cm electrode was 1005 pC, of which $\Delta\{Q_s + Q_{dne}\}$ = 961 pC and ΔQ_{dne} = 44 pC. ΔQ_s measured by electrometer 2 for the 0.5 cm electrode was 1002 pC, of which $\Delta\{Q_s + Q_{dne}\}$ = 769 pC and ΔQ_{dne} = 233 pC. Both electrometers indicated that the discharge occurred in Zone K at 1.36 π rad (with respect to the center of the 2.0 cm electrode, which was assigned to be 0 rad), indicated by ∗ in (a).

instruments.[51,56] We showed, using the RST, that we can measure the number of discharges that occur in different regions of a PS Petri dish. As we discussed above, the four-electrode/two-electrometer configuration of the RST can accurately sense discharges in all regions of the circular path of the sphere. Using this configuration of the RST, we demonstrated that the location of a plasma-oxidized wedge (with an arc of 0.11π rad) on a PS dish can be determined based on our method of locating discharges. We positioned the treated region of the PS dish between two adjacent electrodes, approximately in a zone of overlap (Figure 10a). Four separate experiments were performed with the treated region placed at 0.25π, 0.75π, 1.25π, and 1.75π rad, respectively, relative to the center of the 2.0 cm electrode (assigned as 0π rad). Using the method described in this paper, we were able to determine that the zones with the greatest fraction of discharges always corresponded to the plasma-oxidized region on the PS dish, as expected. This result implies that, if an unknown region of a PS dish were exposed to plasma oxidation, the four-electrode/two-electrometer configuration of the RST, along with our analytical method, can identify the treated region because the number of zones with the most discharges corresponds to that region.

Conclusions

The rolling sphere tool monitors real-time kinetics of contact electrification and makes it possible to analyze patterns of

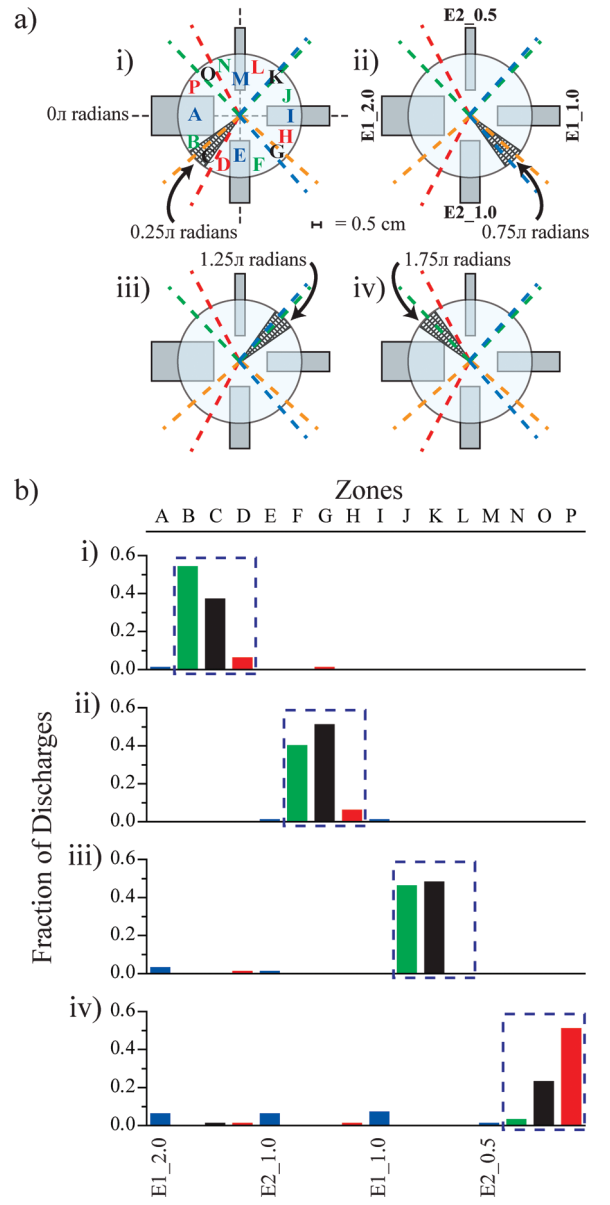

Figure 10. (a) Diagrams representing the four different placements (i−iv) of a plasma-oxidized region (with an arc of 0.11π rad and indicated by the hatch marks) of a PS Petri dish. We used the same four electrode/two electrometer configuration and zone assignation as shown in Figure 9a to demonstrate that the plasma-oxidized region can be identified based on the distribution of discharges. The electrodes are labeled according to the electrometer that they are connected to and their size (e.g., the 2.0 cm electrode connected to electrometer 1 is labeled E1_2.0). (b) A summary of the fraction of discharges that occurred in each zone from the experiments i−iv (diagrammed in (a)) from a steel sphere (d = 3.2 mm) rolling on a PS Petri dish ($T \sim 25$ °C, RH < 10%) in which a 0.11π rad wedge had been plasma-oxidized. In these bar graphs, blue indicates discharges that occurred over an electrode, red indicates those that occurred before an electrode, green indicates those that occurred after an electrode, and black indicates those that occurred in a zone of overlap between adjacent electrodes. Dashed rectangles indicate the zones that had the highest fraction of discharges. As expected, these zones corresponded to where the plasma-oxidized region had been placed.

charging and discharging. By analyzing the peaks/valleys in the charging/discharging curve neighboring each discharge event, we developed a method to determine quantitatively (±0.2π rad) the location of these contact electrification-induced discharges. The method allowed us to analyze the positional distribution of discharges along the circular path of the sphere.

We anticipate that this method will be useful in any field in which the control of electrostatic charging and discharging is important. For example, in the electronics industry, as electronic devices are made smaller, they become more sensitive to ESD. Despite a great deal of effort, ESD still affects many aspects of the industry, including production yields, manufacturing costs, product quality, product reliability, and profitability.[57] Methods of electrostatic control apply to many other industries[58] as well, such as grain handling and storage,[59] chemical and fuel processing and handling,[60,61] and medical engineering (especially in operating rooms).[62,63]

The standard tests used for studying ESD in electronic devices to determine their sensitivity levels involve charging a capacitor using a high-voltage source and then discharging the capacitor through the device or material under investigation.[57] The RST is a simple experimental setup that can be used to study ESD as objects charge in real time, under conditions that are suitable for contact electrification. The ability to study the locations of discharges and analyze their statistical distribution can be useful for evaluating the properties of new materials or patterns in materials in terms of their ability to suppress or trigger discharges.[31,43] Such a system could also be used for identifying types of defects in insulating systems.

Finally, the versatility and simplicity of the RST system combined with the ability to analyze the statistical distribution of discharges will enable physical organic studies of the relationship between molecular structure and discharge behavior. In a separate paper, we will use this method to show that patterning the surfaces of dielectric materials can influence the locations of discharge events due to contact electrification.

Acknowledgment. The Department of Energy, Division of Materials Science and Engineering, under award DE-FG02-00 ER45852 supported the research of S.J.V. Early phases of this work were supported by the Army Research Office with a MURI (W911NF-04-1-0170). We also acknowledge the Xerox Corporation for financial support. X.Z. was funded by the NSF under MRSEC award DMR-0820484. We would also like to thank Prof. Bartosz Gryzbowski (Northwestern University), Dr. Rick Veregan (Xerox Corporation), and Prof. Seth Putterman (UCLA) for helpful discussions.

Supporting Information Available: Figures and the derivation of eq 10. This material is available free of charge via the Internet at http://pubs.acs.org.

References and Notes

(1) Lowell, J.; Rose-Innes, A. C. *Adv. Phys.* **1980**, *29*, 947–1023.
(2) Harper, W. R. *Contact and Frictional Electrification*; Laplacian Press: Morgan Hill, CA, 1998.
(3) Apodaca, M. M.; Wesson, P. J.; Bishop, K. J. M.; Ratner, M. A.; Grzybowski, B. A. *Angew. Chem., Int. Ed.* **2010**, *49*, 946–949.
(4) Pahtz, T.; Herrmann, H. J.; Shinbrot, T. *Nat. Phys.* **2010**, *6*, 364–368.
(5) Shaw, P. E. *Nature* **1926**, *118*, 659–660.
(6) Lowell, J.; Truscott, W. S. *J. Phys. D: Appl. Phys.* **1986**, *19*, 1273–1280.
(7) Lowell, J.; Truscott, W. S. *J. Phys. D: Appl. Phys.* **1986**, *19*, 1281–1298.
(8) Forward, K. M.; Lacks, D. J.; Sankaran, R. M. *Phys. Rev. Lett.* **2009**, *102*, 028001.
(9) Kok, J. F.; Lacks, D. J. *Phys. Rev. E* **2009**, *79*, 051304.
(10) O'Grady, P. F. *Thales of Miletus: The Beginning of Western Science and Philosophy*; Ashgate: Aldershot, UK, 2002.
(11) Camara, C. G.; Escobar, J. V.; Hird, J. R.; Putterman, S. J. *Nature* **2008**, *455*, 1089–1093.
(12) Schein, L. B. *Electrophotography and Development Physics*; Laplacian Press: Morgan Hill, CA, 1996.
(13) Kwetkus, B. A. *Part. Sci. Technol.* **1998**, *16*, 55–68.
(14) Urbakh, M.; Klafter, J.; Gourdon, D.; Israelachvili, J. *Nature* **2004**, *430*, 525–528.
(15) Kaiser, K. L. *Electrostatic Discharge*; Taylor & Francis Group: Boca Raton, FL, 2006.
(16) McCarty, L. S.; Winkleman, A.; Whitesides, G. M. *J. Am. Chem. Soc.* **2007**, *129*, 4075–4088.
(17) Liu, C.-y.; Bard, A. J. *Nat. Mater.* **2008**, *7*, 505–509.
(18) Liu, C.-y.; Bard, A. J. *Chem. Phys. Lett.* **2009**, *480*, 145–156.
(19) Kornfield, M. I. *J. Phys. D: Appl. Phys.* **1976**, *9*, 1183–1192.
(20) Schein, L. B. *Science* **2007**, *316*, 1572–1573.
(21) Veregin, R. P. N.; McDougall, M. N. V.; Hawkins, M. S.; Vong, C.; Skorokhod, V.; Schreiber, H. P. *J. Imaging Sci. Technol.* **2006**, *50*, 282–287.
(22) Veregin, R. P. N.; McDougall, M. N. V.; Hawkins, M. S.; Vong, C.; Skorokhod, V.; Schreiber, H. P. *J. Imaging Sci. Technol.* **2006**, *50*, 288–293.
(23) Harvey, N. E. *Science* **1939**, *89*, 460–461.
(24) Davies, D. K. *Br. J. Appl. Phys.* **1969**, *2*, 1533–1537.
(25) Akande, A. R.; Lowell, J. *J. Phys. D: Appl. Phys.* **1987**, *20*, 565–578.
(26) Liu, C.-y.; Bard, A. J. *J. Am. Chem. Soc.* **2009**, *131*, 6397–6401.
(27) Baytekin, H. T.; Baytekin, B.; Tejerina, B.; Gothard, C. M.; Grzybowski, B. A. Northwestern University, Evanston, IL. Personal communication, 2010.
(28) Baytekin, H. T.; Baytekin, B.; Wesson, P. J.; Grzybowski, B. A. Northwestern University, Evanston, IL. Personal communication, 2010.
(29) Diaz, A. F.; Guay, J. *IBM J. Res. Dev.* **1993**, *37*, 249–259.
(30) McCarty, L. S.; Winkleman, A.; Whitesides, G. M. *Angew. Chem., Int. Ed.* **2007**, *46*, 206–209.
(31) Thomas, S. W., III; Vella, S. J.; Kaufman, G. K.; Whitesides, G. M. *Angew. Chem., Int. Ed.* **2008**, *47*, 6654–6656.
(32) Semenov, O.; Sarbishaei, H.; Sachde, M. *ESD Protection Device and Circuit Design for Advanced CMOS Technologies*; Springer: New York, 2008.
(33) The dielectric strength of an insulating material (or medium) is the maximum electric field strength that it can intrinsically withstand without breaking down. For air at 1 atm of pressure, the dielectric strength is ~30 kV/cm.
(34) Voldman, S. H. *Microelectron. Reliab.* **2004**, *44*, 33–46.
(35) Black, R. A.; Hallet, J. *Am. Sci.* **1998**, *86*, 526–534.
(36) Brown, L.; Burns, D. The ESD Control Process is a Tool for Managing Quality. *Electron. Packag. Prod.* **1990**, 50–53.
(37) Halperin, S. A. ESD Control: Profitable Opportunity in Tight Economic Times. *Threshold*; 2003; Vol. 19, pp 8−9.
(38) Greason, W. D. *IEEE Trans. Ind. Appl.* **1987**, *IA-23*, 205–216.
(39) Gibson, N. *J. Electrost.* **1997**, *40*−*41*, 21–30.
(40) Wiles, J. A.; Grzybowski, B. A.; Winkleman, A.; Whitesides, G. M. *Anal. Chem.* **2003**, *75*, 4859–4867.
(41) Wiles, J. A.; Fialkowski, M.; Radowski, M. R.; Whitesides, G. M.; Grzybowski, B. A. *J. Phys. Chem. B* **2004**, *108*, 20296–20302.
(42) Grzybowski, B. A.; Fialkowski, M.; Wiles, J. A. *J. Phys. Chem. B* **2005**, *109*, 20511–20515.
(43) Thomas, S. W., III; Vella, S. J.; Dickey, M. D.; Kaufman, G. K.; Whitesides, G. M. *J. Am. Chem. Soc.* **2009**, *131*, 8746–8747.
(44) Grzybowski, B. A.; Wiles, J. A.; Whitesides, G. M. *Phys. Rev. Lett.* **2003**, *90*, 083903.
(45) Friedle, S.; Thomas, S. W., III *Angew. Chem., Int. Ed.* **2010**; DOI: 10.1002/anie.201003985.
(46) Alternatively, when the sphere charges negative and the surface charges positive, the valleys become plateaus and the peaks point down.
(47) For example, a steel sphere ($d = 3.2$ mm) rolling on an air-plasma-treated poly(styrene) Petri dish makes a circular path with a circumference of 15 cm. A 1.0 cm-wide (0.4 rad) electrode sensed 90−100% of the charge on the sphere for 0.4 rad (~7%) of the circular path (Zone O). The electrode sensed 10−90% of the charge on the sphere for 1.3 rad (~20%) of the circular path (Zones B and A); the electrode did not sense charge on the sphere for 4.6 rad (~73%) of the circular path (Zone F).
(48) Klein, R. J.; Fischer, D. A.; Lenharat, J. L. *Langmuir* **2008**, *24*, 8187–8197.
(49) Kaczmarek, H.; Kowalonek, J.; Szalla, A.; Sionkowska, A. *Surf. Sci.* **2002**, *507*−*510*, 883–888.
(50) Friedrich, J.; Unger, W.; Lippitz, A.; Koprinarov, I.; Ghode, A.; Geng, S.; Kuhn, G. *Compos. Interfaces* **2003**, *10*, 139–171.
(51) Dupont-Gillain, C. C.; Adriaensen, Y.; Derclaye, S.; Rouxhet, P. G. *Langmuir* **2000**, *16*, 8194–8200.
(52) The rate of charging, and, therefore, the number of discharges, on untreated PS dishes was too low to obtain statistically significant data.
(53) Crowley, J. M. *Fundamentals of Applied Electrostatics*; Laplacian Press: Morgan Hill, CA, 1999.
(54) We determined the total amount of discharge using eq 2. The values for Q_s before and after discharge are calculated using the two maximum values of the peaks (Q_{max}) and the two minimum values in the valleys (Q_{min}) neighboring each discharge event. The errors in the Q_{max} and Q_{min} values

are ±10 pC. Overall, the error in determining the total discharge is ca. ±40 pC, and for an average discharge of 1200 pC, this error represents approximately ±5%.

(55) The contributions of the baseline disruption to the total discharge in these examples are negligible.

(56) Wells, R. K.; Badyal, J. P. S.; Drummond, I. W.; Robinson, K. S.; Street, F. J. *J. Adhes. Sci. Technol.* **1993**, *7*, 1129–1137.

(57) Amerasekera, A.; Verwey, J. *Qual. Reliab. Eng. Int.* **1992**, *8*, 259–272.

(58) Britton, L. G. *Avoiding Static Ignition Hazards in Chemical Operations*; Center for Chemical Process Safety/AIChE: New York, 1999.

(59) Thorpe, D. G. L.; Singh, S.; Cartwright, P.; Bailey, A. G. *J. Electrost.* **1985**, *16*, 193–207.

(60) Leonard, J. T. *Generation of Electrostatic Charge in Fuel Handling Systems: A Literature Survey*; NRL Report 8484; Naval Research Laboratory: Washington D.C., 1981; pp 1−54.

(61) Mellor, A. M.; Baker, P. J. *J. Energ. Mater.* **1994**, *12*, 1–62.

(62) Griffin, N. L. *Am. J. Nurs.* **1953**, *53*, 809–812.

(63) Vickers, M. D. *Br. J. Anaesth.* **1978**, *50*, 659–664.

JP107883U